Chinese Chemical Letters 33 (2022) 3757–3761

Contents lists available at ScienceDirect

Chinese Chemical Letters

journal homepage: www.elsevier.com/locate/cclet

Insight into the role of iron in platinum-based bimetallic catalysts for selective hydrogenation of cinnamaldehyde

Ying Zhang[a,c,1], Jinfang Su[a,b,1], Junnan Chen[a,b], Chengshan Dai[a,b], Bingsen Zhang[a,b,*]

[a] Shenyang National Laboratory for Materials Science, Institute of Metal Research, Chinese Academy of Sciences, Shenyang 110016, China
[b] School of Materials Science and Engineering, University of Science and Technology of China, Shenyang 110016, China
[c] School of Petrochemical Engineering, Liaoning Pertochemical University, Fushun 113001, China

ARTICLE INFO

Article history:
Received 3 September 2021
Revised 8 October 2021
Accepted 25 November 2021
Available online 1 December 2021

Keywords:
Pt_xFe_y NPs
Cinnamaldehyde
Hydrogenation
Chemoselective
IL-TEM

ABSTRACT

Selective hydrogenation of cinnamaldehyde (CAL) toward cinnamyl alcohol (COL) is an extremely important and challenging reaction. Herein, a series of Pt_xFe_y-Al_2O_3 bimetallic catalysts with varied Pt to Fe ratios were prepared by incipient wetness impregnation method. The introduction of Fe significantly modifies the electronic and surface properties of Pt, which clearly enhances the C=O hydrogenation selectivity. Among all the catalysts, Pt_3Fe-Al_2O_3 displays the best catalytic performance and the conversion of CAL is 96.6% with 77.2% selectivity of COL within 1 h. In addition, Pt_3Fe-Al_2O_3 had excellent reusability with 76% COL selectivity after five runs of the recycle process. Further characterization of the fresh, used and cycled catalysts revealed that the structure and electronic state of the synthesized Pt_xFe_y-Al_2O_3 are unchanged after hydrogenation reaction. The identical-location transmission electron microscopy (IL-TEM) results revealed that the interaction between the nanoparticles and the supports was strong and the catalyst was relatively stable.

Selective hydrogenation of cinnamaldehyde (CAL), which contains two functional groups of C=C and C=O bond, to cinnamyl alcohol (COL) is an important and challenging process for producing fine chemicals [1]. However, COL is more difficult to synthesize because the selective hydrogenation of the C=O bond is thermodynamically unflavored [2,3]. In order to increase the selectivity of COL, many efforts and investigations have been made to design and synthesize highly selective and active heterogeneous catalysts. Until now, noble metal catalysts and oxide supports are widely used in catalysis reactions and have excellent activity [4–10]. Nevertheless, the selectivity of CAL to COL is generally low due to the intrinsic properties of Pt [11,12]. This problem can be solved by adding a second metal into Pt to generate a bimetallic catalyst [13,14]. The second metal not only can improve the dispersibility of Pt nanoparticles (NPs), but also can affect the crystallography and electronic structure of Pt NPs, thereby improving the target product selectivity [15–17]. For example, Zhao *et al.* [18] have designed a catalyst, which used the metal-organic framework MIL-101 to encapsulate Pt, for the hydrogenation of α,β-unsaturated aldehydes. The Fe^{3+} and Cr^{3+} in the framework of MIL-101 can regulate the active metal Pt and significantly improve the selectivity to unsaturated alcohol. Chen *et al.* [19] reported that Pt_3Sn/CNTs catalyst prepared by lithium naphthalenide-driven reduction method, which presents excellent catalytic performance because large Pt ensembles were diluted by incorporated Sn atoms and the electron density of Pt was increased. The *in-situ* formed SnO_x interfaces as lewis acid sites facilitate the coordination of C=O bonds, enhancing the selectivity to COL. In our previous work, Pt_xCo_y bimetallic NPs supported on oxygen functionalized CNTs were prepared and the electropositive active sites promote the activation of C=O [20]. However, due to the agglomeration and detachment of $PtCo_3$ NPs, the catalytic activity was decreased during the recycle process.

Despite the widespread investigations, the structural evolution of catalyst under the liquid reaction conditions still remain outstanding challenges. Identical-location transmission electron microscopy (IL-TEM) method is a powerful approach to provide valuable insight into the structural evolution at the same location and the reaction mechanism of catalyst during reaction process [21–23]. Meanwhile, it is possible to explain the structure-performance relationship of catalyst combined its structural characteristics and the catalytic activity [24–26].

* Corresponding author at: Shenyang National Laboratory for Materials Science, Institute of Metal Research, Chinese Academy of Sciences, Shenyang 110016, China.
E-mail address: bszhang@imr.ac.cn (B. Zhang).
[1] These authors contributed equally to this work.

https://doi.org/10.1016/j.cclet.2021.11.077
1001-8417/

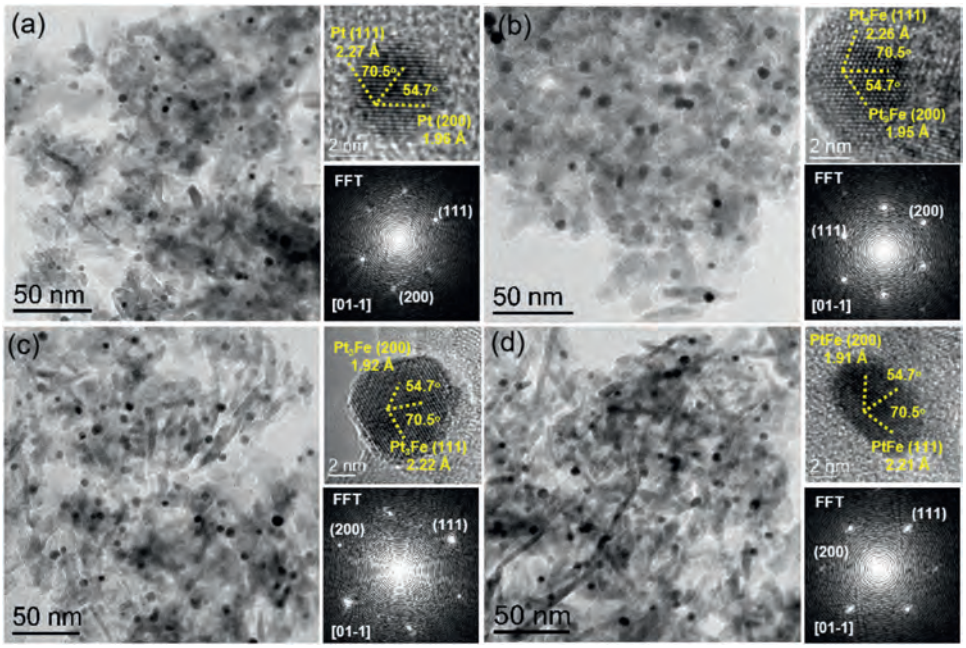

Fig. 1. TEM, HRTEM images (top right) and corresponding FFT (bottom right) of Pt-Al_2O_3 (a), Pt_9Fe-Al_2O_3 (b), Pt_3Fe-Al_2O_3 (c) and PtFe-Al_2O_3 (d), respectively.

In order to synthesize a stable and efficient catalyst, a series of Pt_xFe_y bimetallic catalyst with varied Pt to Fe ratios supported on γ-Al_2O_3 were prepared in this work. The chemoselective hydrogenation of CAL was chosen as probe reaction to explore the influence of second metal Fe in Pt-based catalyst. IL-TEM method was employed to explore the structural evolution during the liquid phase reaction, and the corresponding structure-activity relationship was proposed.

The morphology and structure of the synthesized Pt_xFe_y-Al_2O_3 catalysts were characterized by TEM (Fig. 1 and Fig. S1 in Supporting information). Highly dispersed Pt_xFe_y NPs on Al_2O_3 support can be observed from the low-magnification high-angle annular dark-field scanning TEM (HAADF-STEM) images. The particle size distribution (PSD) histograms of the corresponding NPs (insets of Fig. S1) display that the average particle diameters of Pt_xFe_y NPs are 3.5, 5.3, 5.2 and 4.7 nm regarding Pt-Al_2O_3, Pt_9Fe-Al_2O_3, Pt_3Fe-Al_2O_3 and PtFe-Al_2O_3, respectively. HRTEM images show that the Pt_xFe_y NPs have two crystal planes (200) and (111) with a characteristic acute angle of 54.7°, which belongs to face centered cubic (FCC) structure of Pt. The corresponding Fast Fourier Transform (FFT) patterns also display the structure of Pt_xFe_y NPs and their good crystallinity. With the increase of Fe content, the d-spacing of (200) and (111) gradually decreased, which further confirms the formation of Pt_xFe_y NPs.

Fig. S2 (Supporting information) shows the X-ray diffraction (XRD) patterns of Al_2O_3 support and Pt_xFe_y-Al_2O_3 catalysts. Fig. S2b is the local enlarged drawing curve in the red rectangle of Fig. S2a. The diffraction peaks of Al_2O_3 support match well with the standard XRD pattern (JCPDS No. 46-1131). For Pt-Al_2O_3, the diffraction peaks related to Pt were detected at 2θ = 39.7°, 46.2° and 67.4°, which corresponding to the (111), (200) and (220) crystal planes of Pt with FCC structure (JCPDS No. 01-1311), respectively. The broaden diffraction peak at 39.7° indicates that the size of Pt NPs is small. The particle size calculated based on the Scherrer formula in XRD are 8.7 nm, 9.0 nm, 10.4 nm, and 9.2 nm, respectively, which is slightly difference with the result from TEM. The detailed analysis is discussed in Supporting information. Furthermore, the position of the diffraction peak at 2θ = 39.7°

The real Pt and Fe contents of Pt-Al_2O_3, Pt_9Fe-Al_2O_3, Pt_3Fe-Al_2O_3 and PtFe-Al_2O_3 were determined by inductively coupled plasma mass spectrometry (ICP-MS) and the results are listed in Table S1. Pt contents were examined as 3.85, 4.00, 2.95 and 2.20 wt%, and Fe contents were 0, 0.20, 0.32 and 0.65 wt%, respectively. These measurements indicate that Pt/Fe atomic ratios are approximately close to the desired ratios.

X-ray photoelectron spectroscopy (XPS) was used to further analyze the surface chemical states of Pt. Since Al 2p peak overlaps with Pt 4f peak, which is the most prominent platinum electron line, the Pt $4d_{5/2}$ was analyzed instead (Fig. 2a). It can be seen that the introduction of Fe has a direct impact on the binding energy of Pt 4d, which shifts to higher values slightly with Fe content increased. It indicates that there is electron transfer from Pt to Fe in these bimetallic catalysts. The surface atomic ratio of Pt and Fe on the basis of XPS analysis are listed in Table S1 (Supporting information).

Furthermore, *in-situ* diffuse reflection IR Fourier transform spectroscopy (DRIFTS) of CO as probe molecule was conducted to study the surface properties of Pt_xFe_y-Al_2O_3 catalysts. As shown in Fig. 2b, there are two vibration regions of CO adsorbed on Pt-Al_2O_3 and Pt_9Fe-Al_2O_3 catalysts. The band at about 2095 cm^{-1} is assigned to CO adsorbed on PtO_x sites [27], and the band at around 2065 cm^{-1} is assigned CO linearly adsorbed on the Pt (100) facets [28,29]. For Pt_3Fe-Al_2O_3 and PtFe-Al_2O_3 catalysts, a main CO band at 2084 cm^{-1} and a shoulder band at around 2054 cm^{-1} were detected. The main one could be attributed to the CO linearly absorbed on the Pt(111) planes [29,30], and the shoulder band is ascribed to CO adsorbed on Pt sites at the step edges, corners, and defects [28]. The DRIFTS results indicate that the relativity strong interaction between Pt and Fe occurred in the synthetic process. Moreover, Pt(100) facets are less selective for COL formation than Pt(111) facets [31], so the Pt-Al_2O_3 and Pt_9Fe-Al_2O_3 catalysts may be less selective for COL formation when compared with the other two catalysts.

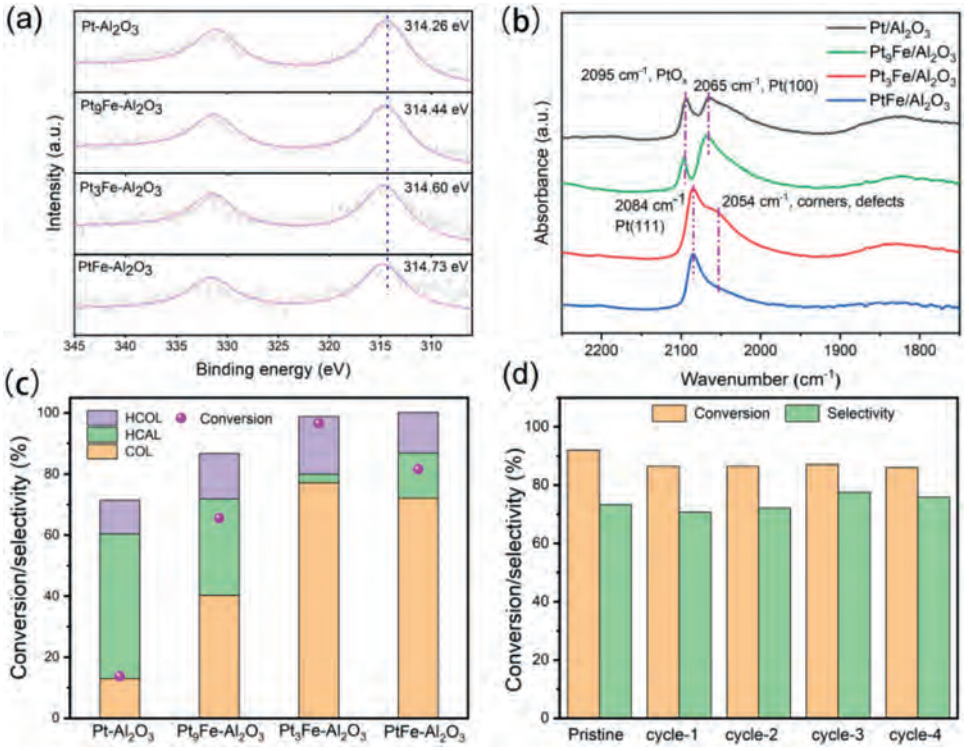

Fig. 2. Pt 4d XPS spectra (a), *in-situ* CO-DRIFTS spectra (b) and catalytic performance of Pt_xFe_y-Al_2O_3 (c) and cycling test of Pt_3Fe-Al_2O_3 for CAL hydrogenation to COL (d). Reaction conditions: T = 80 °C, P = 1.5 MPa, 5 mmol CAL, 30 mg catalysts, 10 mL diethylene dioxide was used as solvent, reaction time: 1 h.gradually shifts to a higher angle with the increase of Fe content (Fig. S2b), which proves that Fe enters Pt lattice and they form platinum iron structure. These results are consistent with the structural features reflected by HRTEM analysis in Fig. 1.

The catalytic performance was evaluated in the selective hydrogenation of CAL over Pt-Al_2O_3, Pt_9Fe-Al_2O_3, Pt_3Fe-Al_2O_3, and PtFe-Al_2O_3 catalysts, as shown in Fig. 2c. The CAL conversion and the COL selectivity gradually increase with the increasing of Fe content. The Pt_3Fe-Al_2O_3 catalyst exhibits the best catalytic performance with 77.2% selectivity to COL at a 96.6% CAL conversion after 1 h of reaction. In contrast, Pt-Al_2O_3 catalyst showed the highest HCAL selectivity and the lowest COL selectivity (13.04%), indicating that pure Pt preferentially hydrogenates the C=C double bond. With the introduction of Fe, the selectivity of COL over Pt_xFe_y-Al_2O_3 catalysts is significantly improved, indicating that the addition of Fe can inhibit the hydrogenation of C=C bonds. It is because the addition of Fe changes the electronic state of Pt, and the electron-deficient Pt is more conducive to the adsorption and hydrogenation of C=O bonds [20]. The catalytic performance decreased with the further increasing of Pt content due to the excess Fe covers the active species of Pt on the surface. That is, the introduction of an appropriate amount of Fe atoms is beneficial to increase the conversion rate of CAL and the selectivity to COL. A comparison of the catalytic performance with some representative reported catalysts for the CAL hydrogenation is listed in Table S2 (Supporting information). Herein, the Pt_3Fe-Al_2O_3 catalyst showed significant advantages in conversion.

The reuse performance is an important factor in evaluating heterogeneous catalysts quality. So the catalyst stability of Pt_3Fe-Al_2O_3 was further investigated based on its excellent catalytic performance. As shown in Fig. 2d, the high selectivity to COL can be basically remained at 76% with a slight decrease (only 6%) of the CAL conversion after five cycles of reaction. It shown that Pt_3Fe-Al_2O_3 catalyst has good stability and can be reused.

The fresh, used and cycled Pt_3Fe-Al_2O_3 catalysts were collected and further characterized by TEM. The analysis on HRTEM images (Fig. 3) of the fresh, used and cycled Pt_3Fe-Al_2O_3 catalysts indicates that the crystal structure of the catalysts remains unchanged. The FFT patterns also prove that the crystal structure is stable. The HAADF-STEM images and the corresponding particle size statistics (Figs. 3d, h, i) exhibit that Pt_3Fe NPs are uniformly dispersed on the Al_2O_3 supports and no particle growth or agglomeration was detected after reusing.

The structure of the fresh, used and cycled Pt_3Fe-Al_2O_3 catalysts were also investigated by XRD (Fig. S3 in Supporting information). The main diffraction peak position of all the Pt_3Fe-Al_2O_3 catalysts are almost same, indicating that the structure of the catalysts did not change. XPS are used to characterize the electronic properties of the catalysts, as shown in Fig. S4 (Supporting information). The Pt 4d binding energy of the used and cycled Pt_3Fe-Al_2O_3 catalysts (314.6 eV) is consistent with that of the fresh catalyst (314.6 eV), indicating that Pt electronic state of the reused (up to five runs) Pt_3Fe-Al_2O_3 catalyst remains unchanged. It proves that the electronic properties of the catalysts are stable after hydrogenation reaction.

IL-TEM method was employed to investigate the structural evolution and stability of the catalysts. The acquired TEM images of fresh, used and cycled Pt_3Fe-Al_2O_3 at identical location are shown in Fig. 4 and Fig. S5 (Supporting information). The morphologies of Al_2O_3 supports are almost same after used and cycled, and most of Pt_3Fe NPs are stable on the Al_2O_3 support after cycling process (marked by red circle). Only very few NPs are detached from the support (marked by yellow circle). The high stability of catalyst is attributed to the strong interaction between Pt_3Fe NPs and support.

In summary, a series of Pt_xFe_y-Al_2O_3 catalysts with varied Pt to Fe ratios were prepared by the incipient wetness impregnation method and tested in the chemoselective hydrogenation of CAL to evaluated their catalytic performance. Due to the electronic and surface properties of Pt can be adjusted by the introduction of Fe,

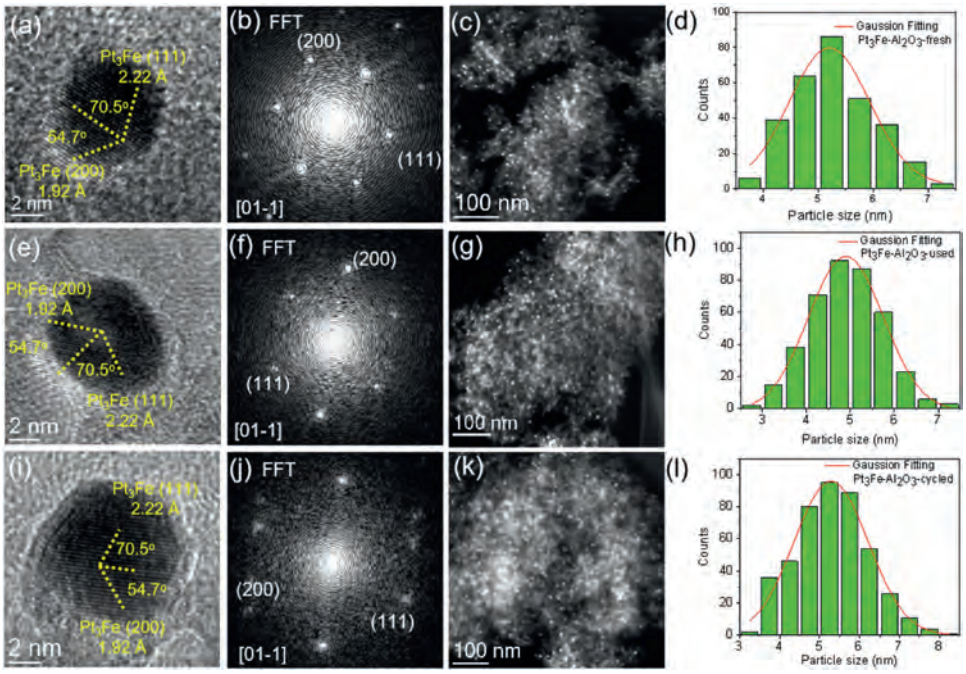

Fig. 3. HRTEM (a, e, i) and corresponding FFT (b, f, j), HAADF-STEM images (c, g, k) and PSD histograms (d, h, l) of fresh (a–d), used (e–h) and cycled (i–l) Pt_3Fe-Al_2O_3 catalyst, respectively.

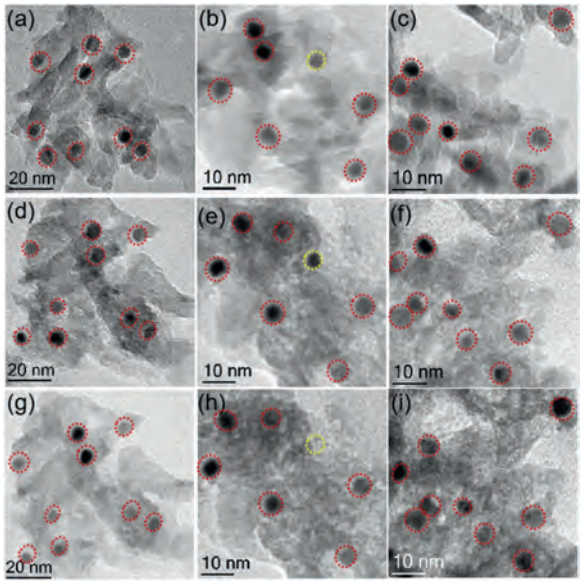

Fig. 4. TEM images at identical location of fresh (a–c), used (d–f) and cycled (g–i) Pt_3Fe-Al_2O_3 catalysts.

the COL selectivity and CAL conversion increased dramatically with the decrease of Pt to Fe ratio. The Pt_3Fe-Al_2O_3 catalyst performs the highest catalytic activity with 77.2% COL selectivity at 96.6% CAL conversion. However, a further increase of the amount of Fe leads to the active sites on the surface are covered by excess Fe, which resulting in decrease in activity. Further characterization of the fresh, used and cycled catalysts revealed that the structure and electronic state of Pt_3Fe NPs were stable. IL-TEM method was conducted to investigate the structural evolution of the catalyst at the identical location under real reaction conditions. The results show that the interaction between the Pt_3Fe NPs and Al_2O_3 support is strong. The stable structure can be maintained after reused, indicating that the prepared Pt_xFe_y-Al_2O_3 catalysts are relatively stable.

Declaration of competing interest

The authors declare that they have no known competing financial interests or personal relationships that could have appeared to influence the work reported in this paper.

Acknowledgments

The authors gratefully acknowledge the financial support provided by the National Natural Science Foundation of China (No. 21773269, 22072164, 21761132025, 51932005) and LiaoNing Revitalization Talents Program (No. XLYC1807175).

Supplementary materials

Supplementary material associated with this article can be found, in the online version, at doi:10.1016/j.cclet.2021.11.077.

References

[1] P. Gallezot, D. Richard, Catal. Rev. Sci. Eng. 40 (1998) 81–126.
[2] X.F. Wang, X.H. Liang, P. Geng, Q.B. Li, ACS Catal. 10 (2020) 2395–2412.
[3] X.C. Lan, T.F. Wang, ACS Catal. 10 (2020) 2764–2790.
[4] X.Q. Xie, Z.J. Wu, N. Zhang, Chin. Chem. Lett. 31 (2020) 1014–1017.
[5] S.P. Wang, S.H. Hou, C. Wu, Y.J. Zhao, X.B. Ma, Chin. Chem. Lett. 30 (2019) 398–402.
[6] Y.Z. Yin, B. Hu, G.L. Liu, X.H. Zhou, X.L. Hong, Acta Phys. Chim. Sin. 35 (2019) 327–336.
[7] J. Zhang, L. Wang, Z.Y. Wu, et al., Acta Phys. Chim. Sin. 36 (2020) 1912001.
[8] H.E. Yu, X. Yang, Y. Wu, et al., J. Energy Chem. 40 (2020) 188–195.
[9] Y.S. Ma, L.Y. Zhang, W. Shi, et al., Chin. Chem. Lett. 20 (2019) 183–186.
[10] Y. Zhang, D.F. Zhang, X.Y. Xu, B.S. Zhang, Chin. Chem. Lett. 29 (2018) 1350–1354.
[11] L. Zhang, M. Zhou, A. Wang, T. Zhang, Chem. Rev. 120 (2020) 683–733.
[12] W. Yu, M.D. Porosoff, J.G. Chen, Chem. Rev. 112 (2012) 5780–5817.
[13] C. Yang, S. Bai, Y. Feng, X. Huang, ChemCatChem 11 (2019) 2265–2269.
[14] A.J. Plomp, D.M.P. van Asten, A.M.J. van Eerden, et al., J. Catal. 263 (2009) 146–154.
[15] Q. Zheng, D. Wang, F. Yuan, et al., Catal. Lett. 146 (2016) 1535–1543.

[16] J. Shi, M. Zhang, W. Du, W. Ning, Z. Hou, Catal. Sci. Technol. 5 (2015) 3108–3112.
[17] N. Zhang, Q. Shao, P. Wang, X. Zhu, X. Huang, Small 14 (2018) 1704318.
[18] M. Zhao, K. Yuan, Y. Wang, et al., Nature 539 (2016) 76–80.
[19] X. Chen, H. Cao, X.Z. Chen, et al., ACS Appl. Mater. Interfaces 12 (2020) 18551–18561.
[20] J.F. Su, W. Shi, X. Liu, et al., J. Catal. 388 (2020) 164–170.
[21] L. Zhang, W. Shi, B. Zhang, J. Energy Chem. 26 (2017) 1117–1135.
[22] W. Shi, B. Zhang, Y. Lin, et al., ACS Catal. 6 (2016) 7844–7854.
[23] D.S. Su, B.S. Zhang, R. Schlögl, Chem. Rev. 115 (2015) 2818–2882.
[24] W. Shi, T. Gao, L. Zhang, et al., Chin. J. Catal. 40 (2019) 1884–1894.
[25] W. Shi, K.-H. Wu, J. Xu, et al., Chem. Mater. 29 (2017) 8670–8678.
[26] T.T. Gao, W. Shi, Y. Zhang, et al., Chem. Eur. J. 26 (2020) 8990–8996.
[27] Y. Chen, J. Lin, L. Li, et al., Appl. Catal. B: No. Environ. 282 (2021) 119588.
[28] Q. Wang, G. Wang, H. Xin, et al., Catal. Sci. Technol. 9 (2019) 3226–3237.
[29] F. Hoxha, B. Schimmoeller, Z. Cakl, et al., J. Catal. 271 (2010) 115–124.
[30] E. Schmidt, W. Kleist, F. Krumeich, T. Mallat, A. Baiker, Chem. Eur. J. 16 (2010) 2181–2192.
[31] S. Kato, J. Ohyama, M. Machida, A. Satsuma, Catal. Sci. Technol. 9 (2019) 2097–2102.